ACS APPLIED MATERIALS & INTERFACES

Research Article

www.acsami.org

Size, Shape-Dependent Growth of Semiconductor Heterostructures Mediated by Ag_2Se Nanocrystals as Seeds

Weiwei Xu,[†,‡] Jinzhong Niu,*[,†,‡] Hongzhe Wang,[†] Huaibin Shen,[†,*] and Lin Song Li[†]

[†]Key Laboratory for Special Functional Materials, Henan University, Kaifeng 475004, P. R. China

[‡]Department of Mathematical and Physical Sciences, Henan Institute of Engineering, Zhengzhou, 451191, P. R. China

Supporting Information

ABSTRACT: Size- and shape-controllable Ag_2Se-ZnS nanorods (NRs) and nanowires (NWs) have been synthesized successfully by the solution−liquid−solid (SLS) method. By using Ag_2Se nanocrystals (NCs) as seeds and catalyst, colloidal Ag_2Se-ZnS NRs and NWs with controllable diameters and lengths in ranges of 5−12 nm and 15−600 nm were successfully synthesized by altering the experimental variables, such as diameter of Ag_2Se NCs, amount of precursor, reaction time, and reaction temperature. The Ag_2Se NCs not only played a key role in the control of the shape of ZnS NCs but also influenced the crystal structure of ZnS NCs. The related surface photovoltage of heterostructured Ag_2Se-ZnS NWs have also been studied and the formation of Ag_2Se-ZnS heterostructure was confirmed. Moreover, this SLS method was successfully exploited to synthesize Ag_2S-ZnS heterostructures.

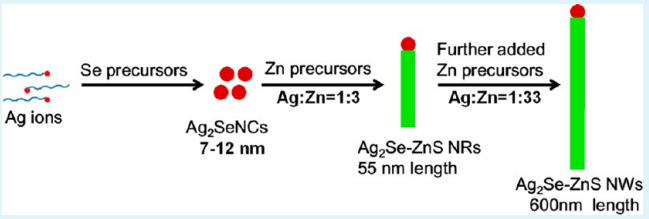

KEYWORDS: *heterostructures, Ag_2Se-ZnS, nanorod/wire, surface photovoltage, solution−liquid−solid*

INTRODUCTION

In the past few years, heterostructured nanomaterials (such as metal−metal, metal−semiconductor, and semiconductor−semiconductor) have attracted much attention because of their great potential in different application fields.[1−8] Because of the flexibility of bandgap engineering, semiconductor−semiconductor heterostructures have been considered to offer better opportunities for internal exciton separation and carrier transport and optoelectronic applications, so the hybrid semiconductor−semiconductor heterostructures is one of the research focuses recently.[9−11]

To date, methods for designing semiconductor−semiconductor heterostructures can be categorized by (i) seed growth method, by which one semiconductor material epitaxially grow on the suitable crystallographic facet offered by the seed semiconductor material, leading to heterostructured nanomaterials. Therefore, a proper lattice mismatch between the growing crystallographic facets of two different types of semiconductor nanomaterials is required, such as CdSe-ZnS,[11] CdTe/CdSe,[12] $Cd_{1-x}Zn_xSe$/ZnSe/ZnS,[13] and Ag_2Te/ZnS.[14] (ii) catalyst-assist growth method, by which one semiconductor nanomaterial is used as a catalyst for growing rod- or wire-shaped semiconductor-semiconductor heterostructures, such as Ag_2S-ZnS,[15,16] Cu_2S-In_2S_3,[17] and Mn-doped Ag_2S-ZnS.[18] As is well-known, Ag_2Se as typical materials with their intrinsic phase transition have attracted much interest because they undergo a reversible transformation between semiconductor and superionic conductor. This unique feature would enable Ag_2Se NCs to potentially be thermoelectric materials, which can play a role in both primary power generation and energy conservation,[19] and ZnS heterostructure has potential at photovoltaic devices.[20]

There are still few reports about the controllable synthesis of Ag_2Se nanocrystals (NCs) and its heterostructures Ag_2Se-ZnS. Therefore, it is important to find a robust method to directly, simply, and quickly synthesize Ag_2Se-ZnS NRs and NWs.

Recently, our group reported the synthesis of Ag-ZnS nanorods (NRs) and nanowires (NWs) by using Ag NCs as seeds and catalyst by solution-liquid−solid (SLS) method.[7] This approach opens a simple, innovative, and repeatable "green" way to prepare metal−semiconductor heterostructured nanomaterials. On the basis of this method and "green" phosphine-free concept,[21−23] we report the synthesis of size- and shape-controllable Ag_2Se-ZnS heterostructured NRs and NWs by SLS method (Scheme 1). The diameter and length of Ag_2Se-ZnS NRs and NWs are controlled by altering the experimental variables, such as diameter of Ag_2Se NCs, amount

Scheme 1. Controlled Synthetic Procedure of Ag_2Se-ZnS NRs and NWs

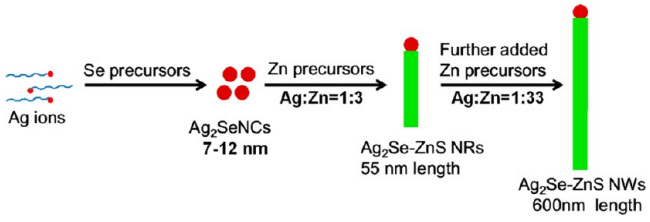

Received: May 15, 2013
Accepted: July 17, 2013
Published: July 17, 2013

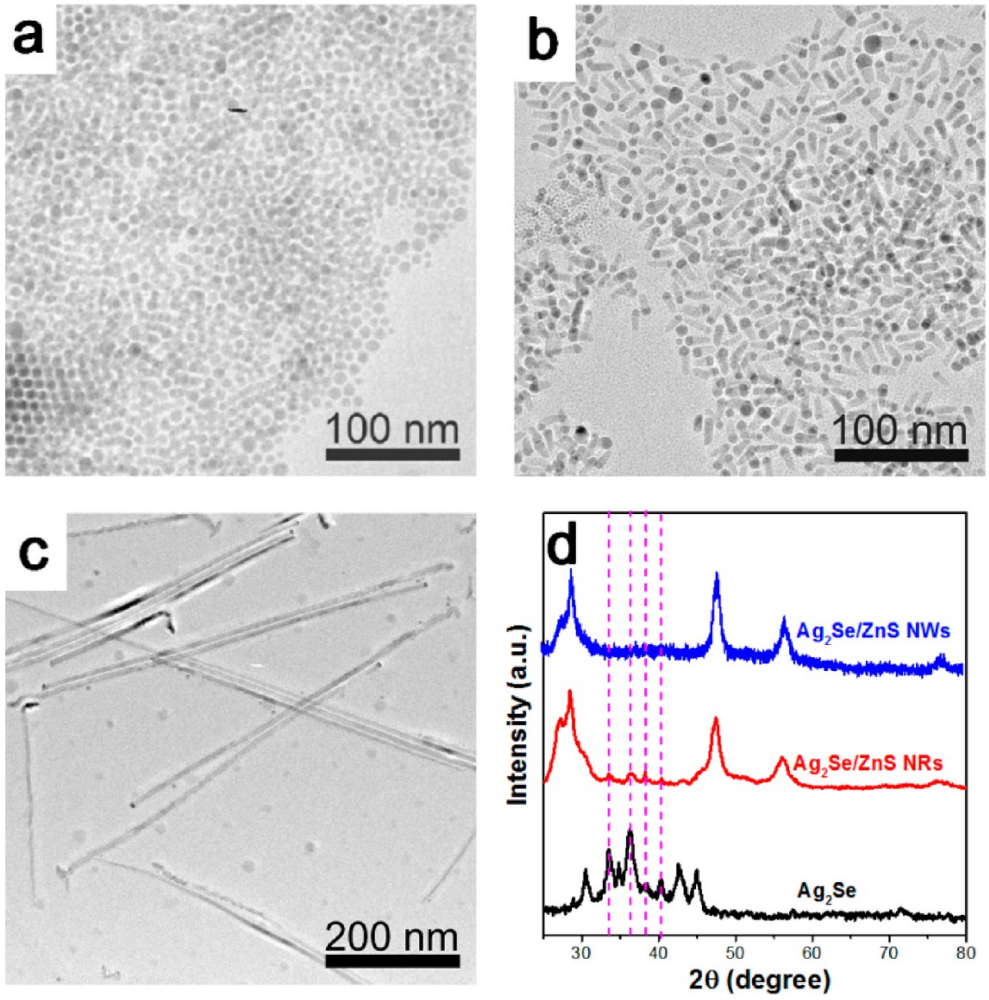

Figure 1. TEM images of (a) 7.5 nm Ag_2Se NCs; (b) Ag_2Se-ZnS NRs with 7.5 nm width and 18 nm length ($mol_{Ag\ precursor}$:$mol_{Zn\ precursor}$ = 1:3 and 30 min reaction times); and (c) Ag_2Se-ZnS NWs with 7.5 nm width and 600 nm length ($mol_{Ag\ precursor}$:$mol_{Zn\ precursor}$ = 1:33 and 33 h reaction times). (d) XRD patterns of Ag_2Se, Ag_2Se-ZnS NRs, and Ag_2Se-ZnS NWs.

of precursor, reaction time, and reaction temperature. The related surface photovoltage (SPV) studies of heterostructured Ag_2Se-ZnS NWs have also confirmed the formation of Ag_2Se-ZnS heterostructure. The result may lead to some potential applications in photovoltaic cells.

EXPERIMENTAL SECTION

Chemicals. 1-Dodecanethiol (DDT, 98%), oleic acid (OA, 90%), selenium (Se, 99.99%), 1-octadecene (ODE), and zinc oxide (ZnO, 99.99%, powder) were purchased from Aldrich. 2,4-Pentanedione (acac, 98%), triethylamine (99%), hexanes (analytical grade), methanol (analytical grade), ethanol (analytical grade), and acetone (analytical grade) were purchased from Tianjin Chemical Reagents Co. Ltd. Silver nitrate ($AgNO_3$, 99.8%) and paraffin oil (analytical grade) were obtained from Beijing Chemical Reagents Co. Ltd. All the chemicals were used as received without any further purification.

Synthesis of Agacac. In a typical synthesis, 20 mmol $AgNO_3$ was dissolved in 10 mL of deionized water. Under magnetic stirring, 2,4-pentanedione (5 mL, 50 mmol) was added and kept stirring for 5 min. Agacac was precipitated after appropriate amount of triethylamine was added in the solution. Then, Agacac was washed for several times by ethanol and water, and finally was dried under low temperature.

Stock Solutions for Se, S, and Zn Precursors. Se precursor: It was made by degassing Se (1.578 g, 20 mmol) and 200 mL of ODE in a 500 mL three-neck flask, then the mixture was heated to 220 °C for 180 min under nitrogen flow. During this process, the color of the precursor changed from transparent to orange, red, and finally turned into yellow. S precursor: The sulfur precursor solution (0.1 M) was prepared by heating a mixture of sulfur (0.96 g, 30 mmol) and ODE (300 mL) to 150 °C under nitrogen. Zn precursor: A mixture of ZnO (0.729 g, 9 mmol), oleic acid (44 mmol, 12.42 g), and 16.2 mL paraffin oil were loaded in a 50 mL three-neck flask and heated to 300 °C under nitrogen to obtain a colorless clear solution.

Synthesis of Ag_2Se-ZnS NRs and NWs. For the synthesis of Ag_2Se NCs, Agacac (0.0414 g, 0.2 mmol) was mixed with 8 mL DDT and heated to 130−200 °C under stirring and nitrogen flow for 10 min. Then 2 mL Se precursor was injected into the above flask for the synthesis of Ag_2Se NCs. Finally, a clear dark brown solution containing Ag_2Se NCs was obtained, and then 2 mL of Zn precursor was add into the solution for the growth of ZnS. The temperature was set at 220 °C under a nitrogen flow. After the reaction lasted for 3 h, Ag_2Se-ZnS NRs were synthesized. Then the continuous further addition of Zn precursor resulted the formation of longer Ag_2Se-ZnS NWs (2 mL of Zn precursor was added after every 3 h).

Synthesis of Ag_2S-ZnS NRs. Ag_2S-ZnS NRs were prepared following the same procedures as described above for Ag_2Se-ZnS NRs except the Se precursor was replaced by S precursor.

Characterization. X-ray diffraction (XRD) studies of NCs were carried out with a Philips X′ Pert Pro X-ray diffractometer using Cu Kα radiation (wavelength = 0.154 nm). The specimens were prepared as follows: about 20 mg of purified NCs were dissolved in 0.5 mL toluene and dropped on a low-scattering quartz sample-holder, then it was dried in air and kept overnight in a vacuum desiccator. To get

dx.doi.org/10.1021/am4018303 | ACS Appl. Mater. Interfaces 2013, 5, 7537−7543

better signal-to-noise ratio, the XRD data were collected at a scan rate of 16 s with 0.2° per step. Transmission electron microscopy (TEM) studies were performed using a JEOL JEM-2010 electron microscope operating at 200 kV. X-ray photoelectron spectrum (XPS) measurements were performed on an AXIS ULTRA X-ray photoelectron spectroscope, using monochromatised Al Kα radiation with an anode voltage of 15 kV and emission current of 3 mA. Energy-dispersive X-ray spectroscopy (EDX) studies were preformed on a Hitachi S-3400N scanning electron field-emission microscope.

Kelvin Probe Measurements. A commercial Kelvin probe system (KP-6500 Digital Kelvin Probe System, McAllister Technical Services) was integrated with a light source to determine the work function changes. This apparatus measures the contact potential difference (CPD) between a reference plate and the sample's surface. CPD is defined as the work function of the reference plate connected to the preamplifier minus the work function of the sample, that is, $\varphi_m - \varphi_{sam}$ (where φ_m is the work function of the reference plate (a constant), and φ_{sam} is the work function of the sample). By comparing the work function before and after deposition of Ag_2Se or Ag_2Se-ZnS onto ITO substrate, the change in work function, $\Delta\varphi_m$, after the deposition is obtained. The probe plate is made of stainless steel with a diameter of 4 mm. It was electrically connected via ground to the sample during the measurement. The typical distance between the reference plate of the probe and the sample was less than 1 mm. The oscillation frequency of the probe was 105 Hz.

Surface Photovoltage Spectroscopy (SPS). For SPV response, the samples were illuminated from the backside of transparent substrate by monochromatic light, which was obtained by passing light from a 450-W xenon lamp through a monochromator (IHR 320). SPV spectra were obtained by scanning the wavelength of the incident light from the visible to UV range (250–800 nm) at a typical scanning rate of 30 nm/min. The raw SPV data were not corrected for the spectrum of the xenon lamp.

RESULTS AND DISCUSSION

For the synthesis of Ag_2Se NCs, Agacac was introduced as Ag precursor, DDT was chosen as the surface-capping agent, and Se powder was dissolved in ODE as the Se precursor. By this approach, Ag_2Se NCs with tunable sizes were easily synthesized by adjusting the reaction temperatures. Figure S1 in the Supporting Information shows the lattice spacing of typical HRTEM images for 12 nm Ag_2Se NCs is 0.212 nm corresponding to (113) plane. Table S1 in the Supporting Information displays the measured lattice spacing based on the rings in selected-area electron diffraction (SAED) and compares them to the known lattice spacing for bulk Ag_2Se along with their respective (hkl) indexes (JCPDS, 24–1041). In fact, the Ag_2Se NCs XRD patterns have both the orthorhombic (JCPDS, 24–1041) and cubic (JPCDS 76–0135) phases (see Figure S3 in the Supporting Inforation).

After the addition of Zn precursor to the solution containing preprepared Ag_2Se NCs at elevated temperatures, the Zn precursor reacted with DDT to form Ag_2Se-ZnS NRs and NWs with Ag_2Se on the head. Figure 1 shows the TEM images of Ag_2Se-ZnS NRs ($mol_{Ag\ precursor}$:$mol_{Zn\ precursor}$ = 1:3 and 30 min reaction time) and Ag_2Se-ZnS NWs ($mol_{Ag\ precursor}$:$mol_{Zn\ precursor}$ = 1:33 and 33 h reaction time) after the addition of different amounts of Zn precursor to the solution containing 7.5 nm Ag_2Se NCs with a growth temperature of 220 °C. Without the participation of Ag_2Se NCs in the reaction solution, Zn precursor reacted with DDT to form ZnS NCs (see Figure S2 in the Supporting Information). This indicated that the Ag_2Se NCs played an important role in controlling the shape of the ZnS NCs. Interestingly, the existence of Ag_2Se NCs also influenced the crystal structures of ZnS NCs. Zinc blende structured ZnS NCs were formed without the existence of Ag_2Se seeds (see Figure S2 in the Supporting Information), whereas wurtzite-structured Ag_2Se-ZnS NRs or NWs (Figure 1d, JCPDS 05–0492) were formed if the reaction solution containing preprepared Ag_2Se NCs.

Further HRTEM studies were carried out to obtain detailed information on the orientation relationship between Ag_2Se NCs and ZnS NRs. The HRTEM images of Ag_2Se-ZnS interface and the different selected-area fast Fourier transform (FFT) images are shown in Figure 2a. On the basis of the

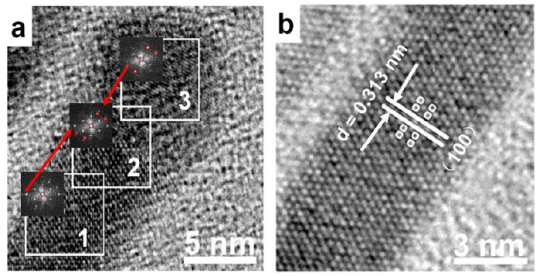

Figure 2. (a) HRTEM image of Ag_2Se-ZnS NRs. The insets FFT images show the area of (1) ZnS, (2) Ag_2Se-ZnS conjunction, and (3) Ag_2Se head. (b) HRTEM image of the section of the ZnS NRs.

analysis of the corresponding crystal lattices, the ZnS rod consists of the (100) plane of wurtzite ZnS NCs (Figure 2a, inset 1), the conjunction interface consists of the (113) plane of the Ag_2Se NCs and the (100) plane of the ZnS rods (Figure 2a, inset 2), the Ag_2Se head consists of the (113) plane of the Ag_2Se NCs (Figure 2a, inset 3), and the preferential growth of ZnS NRs is along the direction of the (100) plane. The (100) plane of ZnS is further confirmed by a higher quality HRTEM image (Figure 2b), which is strong evidence that d = 0.313 nm corresponds to the (100) plane of hexagonal ZnS.

XPS was performed to investigate the chemical composition of the Ag_2Se NCs and Ag_2Se-ZnS NRs. High-resolution spectra of Ag 3d, Se 3d, Zn 2p, and S 2p were measured to determine the oxidation states of the constituent elements. Figure 3a shows the Ag 3d splitting into Ag $3d_{5/2}$ and Ag $3d_{3/2}$ which indicates that the oxidation state of Ag ion is univalent, and with the growth of ZnS rods the proportion of Ag decreases. The Se $3d_{5/2}$ peak is located at 54.1 eV, indicating the existence of Se^{2-} (Figure 3b). Two peaks located at 160.1 and 161.3 eV in Figure 3c are assigned to S 2p binding energy with a valence of −2, which is the characteristic of sulfide. It is also noted that the signal of sulfur element increased greatly after the reaction, which indicates the formation of ZnS NRs. The peaks of Zn 2p appear at binding energies of 1020.1 and 1043.2 eV, which can be assigned to Zn(II) with a peak splitting of 23.1 eV (Figure 3d). Meanwhile, EDX was also measured to further study the elemental composition and purity of these as-obtained NCs. The EDX results undoubtedly demonstrate that the chemical components mainly consisted of Ag and Se for the as-obtained NCs. It is also noted that a few sulfur element is detected in EDX spectra of Ag_2Se NCs (see Figure S4a in the Supporting Information), which is likely originated from the thiol capping ligands on the surface (the other detected elements Cu and C originated from the carbon-coated copper grid used for the TEM analysis). The great increase in the content for Zn and S (Figure S4b in the Supporting Information) also prove the growth of ZnS NRs.

Figure 4 shows the TEM images of Ag_2Se-ZnS NRs grown on the 7.5 nm sized Ag_2Se NCs with the molar ratio of Ag:Zn

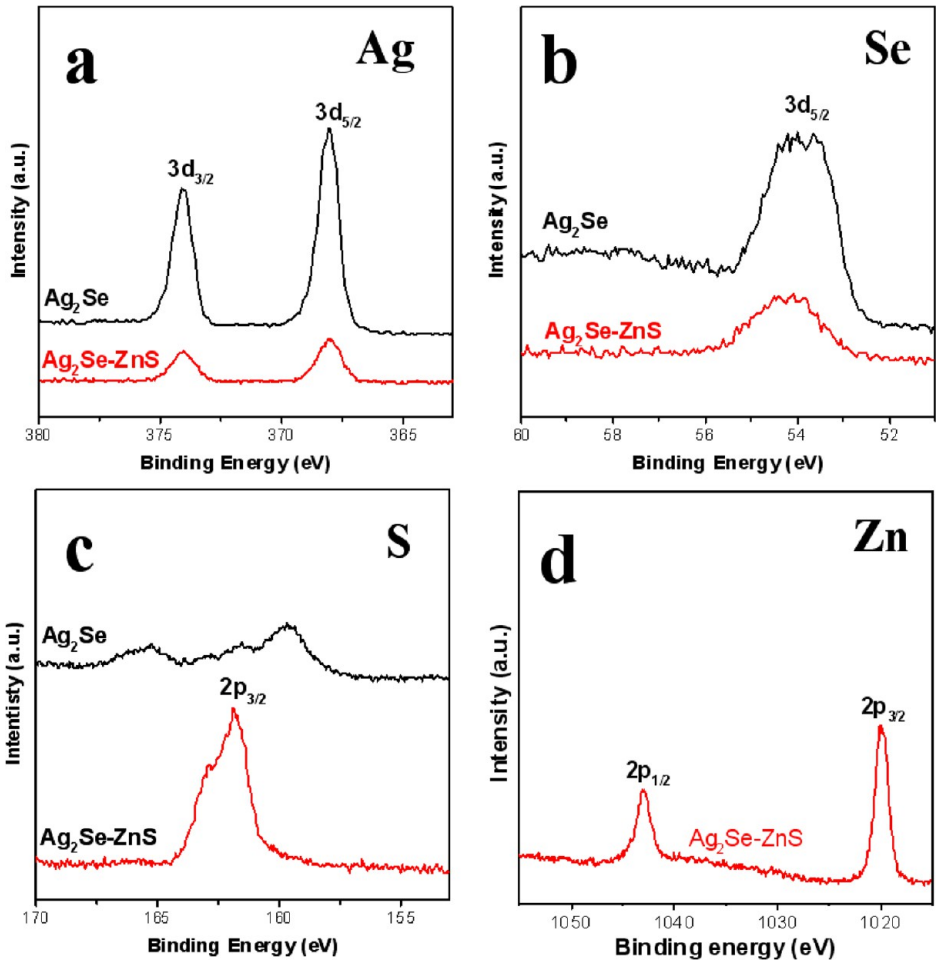

Figure 3. High-resolution XPS spectra of Ag_2Se NCs and Ag_2Se-ZnS NRs.

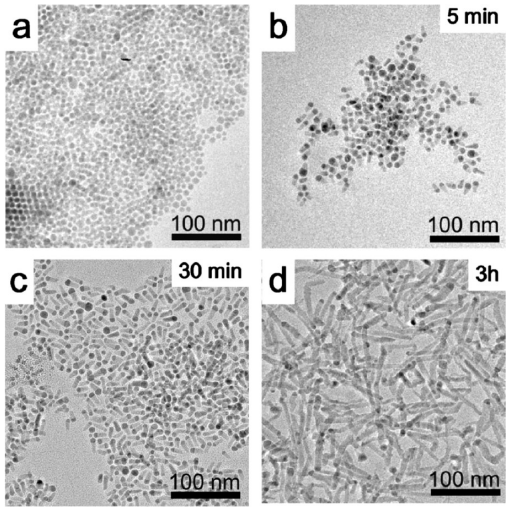

Figure 4. TEM images of the temporal morphology evolution of (a) Ag_2Se NCs, (b–d) Ag_2Se-ZnS NRs with different reaction times.

about 1:3. After the reaction lasted for 5 min, the short Ag_2Se-ZnS rods with an average length of 12 nm were prepared (Figure 4b). When the reaction lasted for 30 min, the rod length was between 18 and 27 nm (Figure 4c). Further growth consumed the remaining precursors and a final rod length between 40 and 80 nm was obtained when the reaction proceeded for 3 h (Figure 4d). While, in the whole growth process, the rod diameter was kept at about 7.5 nm, without any change was observed. Therefore, the reaction time has an obvious influence on the rod length, but a negligible effect on the rod diameter of the Ag_2Se-ZnS NRs.

The aforementioned synthesis could only achieve Ag_2Se-ZnS NRs with lengths under 100 nm, which is limited by the amount of precursor. Here the effect of the amount of precursor is further studied, same sized (7.5 nm) Ag_2Se NCs were chosen to grow Ag_2Se-ZnS NRs with different amounts of Zn precursor. Figure 5 shows the TEM images of final Ag_2Se-ZnS NWs with 2.4 mmol (Figure 5a needs 12 h for reaction) and 6.6 mmol (Figure 5b needs 33 h for reaction) Zn precursor. The average lengths of NWs are 200 and 600 nm, respectively. It is clearly shown that the diameter of Ag_2Se-ZnS

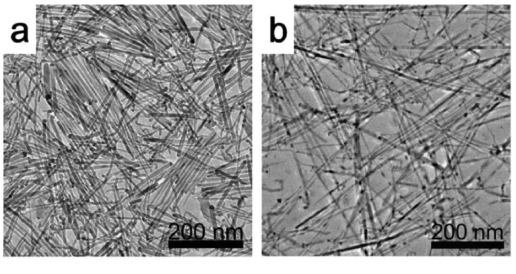

Figure 5. TEM images of as-synthesized Ag_2Se-ZnS NWs when the amounts of Zn precursor are (a) 2.4 and (b) 6.6 mmol.

dx.doi.org/10.1021/am4018303 | ACS Appl. Mater. Interfaces 2013, 5, 7537–7543

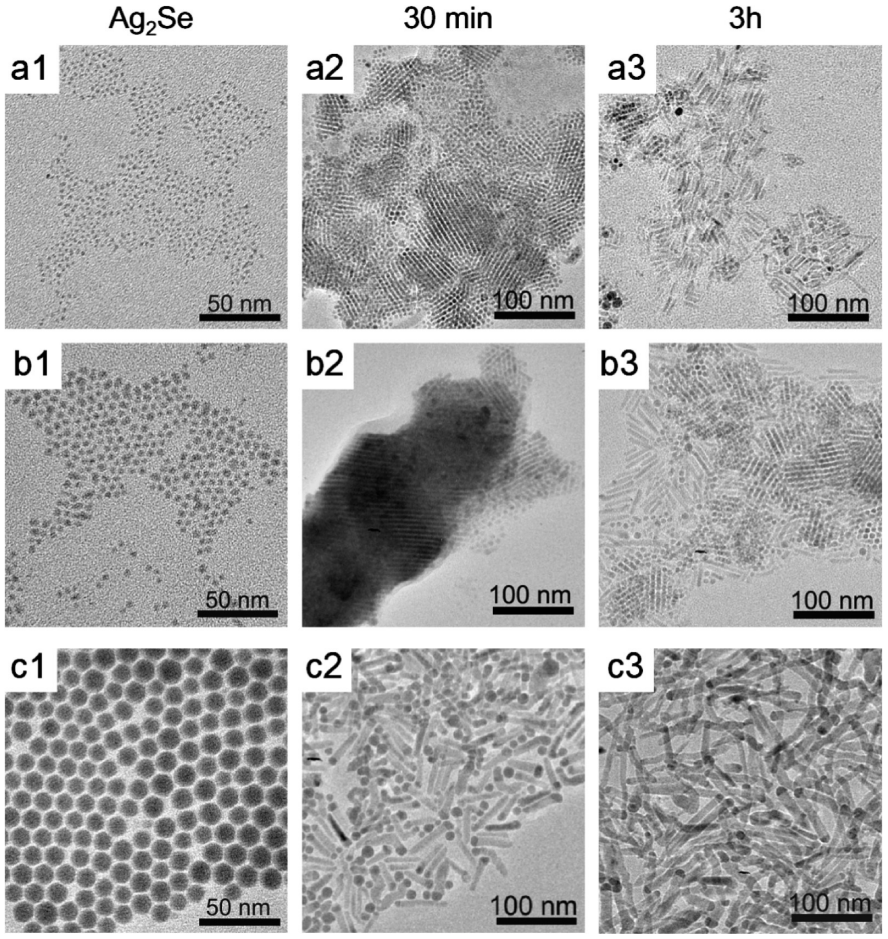

Figure 6. TEM images of the temporal morphology evolution of Ag_2Se-ZnS NRs grown on (a) 2.2, (b) 4.5, and (c) 12 nm Ag_2Se NCs.

NWs is kept the same as the diameter of Ag_2Se NCs in the entire reaction. This indicates that the amount of precursor only affects the length of the rods and wires. A higher quantity of Zn precursor favors the formation of longer rods and wires.

Since the reaction time only influenced the rod length of Ag_2Se-ZnS NRs while the diameter was kept the same with the preprepared Ag_2Se NCs, we inferred that the rod diameter could be influenced by the size of preprepared Ag_2Se NCs. To test this hypothesis, we chose 2.2 nm, 4.4 nm, and 12 nm sized Ag_2Se NCs (Figure 6a–c and Figure S5 in the Supporting Information) to grow Ag_2Se-ZnS NRs. Figure 6a2 shows the TEM image of the reaction product after the addition of Zn precursor for 30 min to the preprepared 2.2 nm Ag_2Se NCs solution. From the image, the size of Ag_2Se-ZnS nanocones increased to 5 nm and had a good self-assembly structure.[24] Further growth resulted uniform Ag_2Se-ZnS NRs after the reaction lasted for 3 h with most of the precursors were consumed, no further growth was observed and the final length of the Ag_2Se-ZnS NRs were between 16 and 34 nm with the diameter maintained at 5 nm (Figure 6a3).

Figure 6b1–3 show the TEM images of products grown on 4.5 nm sized Ag_2Se NCs. Ag_2Se-ZnS NRs were formed with a diameter of 5 nm (Figure 6b2) after the addition of Zn precursor for 30 min, and had a good self-assembly structure.[24] When the reaction lasted for 3 h, the final NRs were formed with a diameter of 5 nm and length of 16–45 nm. Figure 6c1–3 shows the TEM images of products grown on 12 nm sized Ag_2Se NCs. After the addition of Zn precursor, Ag_2Se-ZnS NRs were formed with a diameter of 12 nm and length of 20–55 nm (Figure 6c2) at 30 min, and a diameter of 12 nm and length of 70–180 nm at 3h.

After all, we can conclude that the diameter of Ag_2Se-ZnS NRs and NWs could be controlled by the preprepared Ag_2Se NCs. When the size of Ag_2Se NCs was smaller than 5 nm, the diameters of seed grew Ag_2Se-ZnS NRs were all of 5 nm. We speculate that Ag_2Se NCs undergo Ostwald ripening process and grow to 5 nm because we can only observe 5 nm dot-shaped NCs and hardly observe rod-shaped NCs in Figure a2 and b2. After that 5 nm diameter of Ag_2Se-ZnS NRs were formed. Whereas if the diameter of preprepared Ag_2Se NCs was larger than 5 nm, this seed size determined the diameter of subsequent Ag_2Se-ZnS NRs, the further growth only changed the rod length, and the diameter was kept the same as the preprepared Ag_2Se NCs in the whole reaction process.

Besides the reactants quantities, it was also found that the reaction temperature could significantly influence the reaction kinetics and the obtained products. The reaction products synthesized at different temperatures with all the other reaction conditions unchanged are shown in Figure 7. When the reaction temperature was set of 180 °C, Ag_2Se-ZnS NRs were formed after 30 min of reaction (Figure 7a1), and the length of Ag_2Se-ZnS NRs could reach 32 nm when the reaction last for 3 h (Figure 7a2). When the reaction temperature was set to 270 °C, the length of Ag_2Se-ZnS NRs could reach 100 nm after only 30 min of reaction (Figure 7b1), this was much sooner than reactions which were conducted at 180 °C (Figure 7a1

dx.doi.org/10.1021/am4018303 | ACS Appl. Mater. Interfaces 2013, 5, 7537–7543

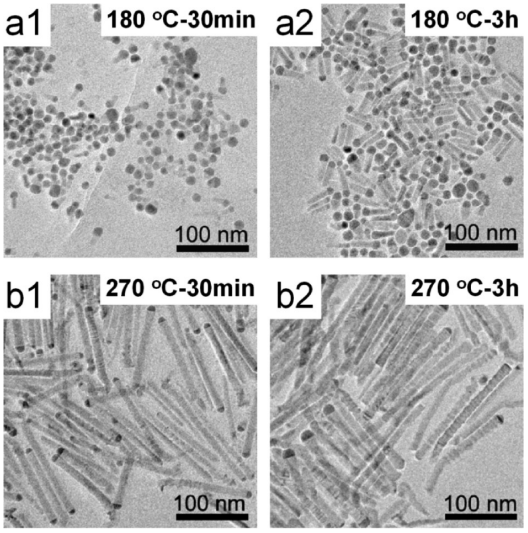

Figure 7. TEM images of Ag_2Se-ZnS NRs at different reaction temperatures and times.

and 7a2) and 220 °C (Figure 4c, d). It is obvious that the reaction temperature influenced the reaction speed and that higher temperature favors quick growth of NRs and NWs.

SPV and SPS are very sensitive tools for studying the change of charge distribution on semiconductor surfaces, buried interfaces, and heterojunctions.[25−29] To better understand photo response properties, we measured the SPV spectra for ITO, Ag_2Se/ITO junction, and Ag_2Se-ZnS/ITO junction. These are the optical absorption bands followed by charge transfer across the interface and contribute to the photovoltaic effect. For reference purpose, bare ITO SPS was employed as a calibration baseline. We found a broad peak at 310 nm with a peak value of 80 mV, which should belong to the bandgap excitation of ITO (E_g = 3.7−4.3 eV).[30] The negative photovoltaic response indicates a typical n-type material with an upward band bending near the surface.

After the deposition of Ag_2Se NCs to form Ag_2Se/ITO junction, the work function value increased with the increase of the length of NWs (Figure 8a), but the shape and position of the SPS peak did not change. There is no SPV response for Ag_2Se NCs from visible range to NIR range (400 to 1400 nm). Therefore, Ag_2Se NCs showed metallic behavior in its electronic conductivity due to a coexistence of both orthorhombic phase (which has a band gap of ∼0.098 eV) and cubic phase (which is metallic).[19,31] Such Ag_2Se/ITO junction does not change the initial band bending formed on ITO, therefore, SPV response almost keep unchanged. After the growth of ZnS on Ag_2Se NCs, a semiconductor behavior is formed on Ag_2Se-ZnS NWs, and their SPV spectra of Ag_2Se-ZnS NWs with 80, 200, and 600 nm lengths have been collected and shown in Figure 8, respectively. With the increase in Ag_2Se-ZnS NWs length, the band gap of ZnS NWs decreased and this conducted a decrease of work function value. When the length of heterostructured Ag_2Se-ZnS NWs increased to over 200 nm, a new SPV response located at 340 nm begin to appear, this is related to the band gap of wurtzite structured ZnS (E_g = 3.80 eV) directly. The longer ZnS NWs was synthesized, the clearer such SPV peak was observed. This phenomenon was also corresponding to the absorption peaks located around 325 nm (see Figure S6 in the Supporting Information). Compared to the pristine ZnS NCs, we found that work function of Ag_2Se-ZnS NWs was higher than ZnS NCs and ITO (see Figure S7 in the Supporting Information). However, we can adjust work function of ZnS nanomaterial through the growth of Ag_2Se-ZnS NWs which is useful in photovoltaic cell.

Furthermore, this SLS method was also exploited to synthesize Ag_2S-ZnS NRs (see Figures S8−S10 in the Supporting Infomration). The resulting Ag_2S-ZnS NRs have a typical length of 60−150 nm and width with diameter of 8 nm (Figure 9a). HRTEM image shows the conjunction interface consists of the (121) plane of the Ag_2S NC and the (101) plane of the ZnS rod (Figure 9b) clearly. According to the XRD patterns, the resulting Ag_2S-ZnS NRs also have wurtzite structure (see Figure S7 in the Supporting Information, JCPDS 05−0492). And more, the reaction temperature significantly influenced the reaction kinetics and morphology of Ag_2S-ZnS heterostructures NWs, and 220 °C is the most suitable temperature for the synthesis of Ag_2S-ZnS NRs and NWs. As shown in Figures S9 and S10 in the Supporting Information, the growth is largely limited at 180 °C, whereas 270 °C broke the heterostructure and separated Ag_2S and ZnS were obtained.

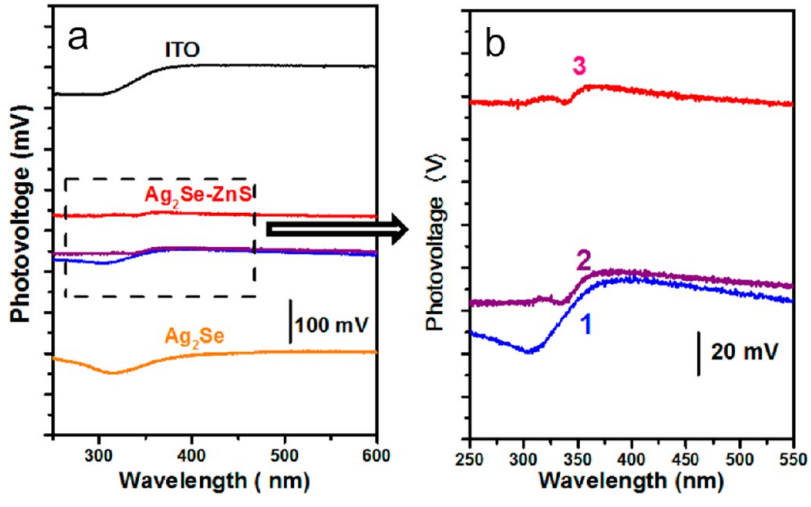

Figure 8. SPV responses for (a) ITO, Ag_2Se, and Ag_2Se-ZnS and (b) Ag_2Se-ZnS NWs with (1) 80, (2) 200, and (3) 600 nm lengths, respectively.

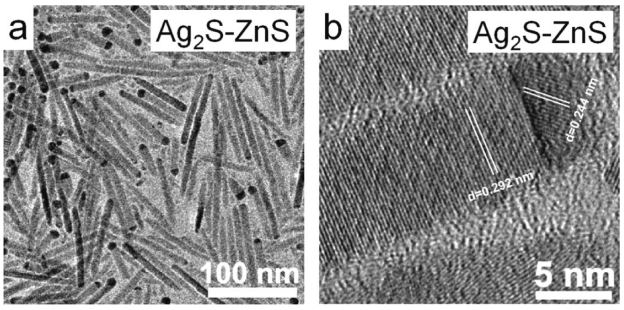

Figure 9. (a) TEM and (b) HRTEM images for Ag_2S-ZnS NRs that reacted for 3 h at 220 °C by using Ag_2S NCs as seeds.

CONCLUSIONS

In this paper, we report the synthesis of size- and shape-controllable Ag_2Se-ZnS heterostructured NRs and NWs by SLS method. Ag_2Se NCs, which acted as seeds and catalysts for the growth of ZnS NRs and NWs, were synthesized by using organometallic Agacac as precursor and tunable particle sizes were obtained by adjusting the reaction temperature. By using Ag_2Se NCs as seeds, we synthesized high-quality colloidal Ag_2Se-ZnS NRs and NWs having purposefully controlled diameters in the range of 5−12 nm and with length of 15−600 nm. The Ag_2Se NCs not only played a key role in the control of the shape of ZnS NCs but also influenced the crystal structure of ZnS NCs. Moreover, the width and length of Ag_2Se-ZnS NRs and NWs were controllable by altering the experimental variables, such as the amount of precursor, reaction time and temperature, and diameter of Ag_2Se NCs. Clear SPV responses can be observed in heterostructured Ag_2Se-ZnS NWs. Furthermore, this SLS method was exploited to synthesize Ag_2S-ZnS NRs.

ASSOCIATED CONTENT

Supporting Information

HRTEM and SAED of Ag_2Se NCs; TEM and SAED of ZnS NCs, EDX, XRD; size histograms of Ag_2Se NCs and Ag_2Se-ZnS NRs; XRD, TEM, and size histograms of and Ag_2S-ZnS NRs. This material is available free of charge via the Internet at http://pubs.acs.org.

AUTHOR INFORMATION

Corresponding Author

*E-mail: niujinzhong@gmail.com (J.N.); shenhuaibin@henu.edu.cn (H.S.). Fax: +86-378-3881358.

Notes

The authors declare no competing financial interest.

ACKNOWLEDGMENTS

This work was financially supported by the research project of the National Natural Science Foundation of China (21071041 and 21201055), Program for Changjiang Scholars and Innovative Research Team in University (PCS IRT1126), Program for New Century Excellent Talents in University of Chinese Ministry of Education (NCET-09-0119), and Natural Science Research Program of Henan Educational Committee, China (12A430003).

REFERENCES

(1) Mokari, T.; Rothenberg, E.; Popov, I.; Costi, R.; Banin, U. *Science* **2004**, *304*, 1787−1790.
(2) Ma, X.; Zhao, Y.; Jiang, X.; Liu, W.; Liu, S.; Tang, Z. *ChemPhysChem* **2012**, *13*, 2531−2535.
(3) Wang, D.; Li, Y. *Adv. Mater.* **2011**, *23*, 1044−1060.
(4) Liu, J.; Qiao, S. Z.; Hu, Q. H.; Lu, G. Q. *Small* **2011**, *7*, 425−443.
(5) Yang, J.; Zhou, Y.; Zheng, S.; Liu, X.; Qiu, X.; Tang, Z.; Song, R.; He, Y.; Ahn, C. W.; Kim, J. W. *Chem. Mater.* **2009**, *21*, 3177−3182.
(6) Cozzoli, P. D.; Pellegrino, T.; Manna, L. *Chem. Soc. Rev.* **2006**, *35*, 1195−1208.
(7) Shen, H.; Shang, H.; Niu, J.; Xu, W.; Wang, H.; Li, L. S. *Nanoscale* **2012**, *4*, 6509−6514.
(8) Tang, Z.; Podsiadlo, P.; Shim, B. S.; Lee, J.; Kotov, N. A. *Adv. Funct. Mater.* **2008**, *18*, 3801−3808.
(9) Talapin, D. V.; Koeppe, R.; Gotzinger, S.; Kornowski, A.; Lupton, J. M.; Rogach, A. L.; Benson, O.; Feldmann, J.; Weller, H. *Nano Lett.* **2003**, *3*, 1677−1681.
(10) Dong, A.; Tang, R.; Buhro, W. E. *J. Am. Chem. Soc.* **2007**, *129*, 12254−12262.
(11) Zaman, B.; Bardelang, D.; Prakesch, M.; Leek, D. M.; Naubron, J.; Chan, G.; Wu, X.; Ripmeester, J. A.; Ratcliffe, C. I.; Yu, K. *ACS Appl. Mater. Interfaces* **2012**, *4*, 1178−1181.
(12) Khatun, Z.; Nurunnabi, M.; Cho, K. J.; Lee, Y. *ACS Appl. Mater. Interfaces* **2012**, *4*, 3880−3887.
(13) Chen, C.; He, X.; Gao, L.; Ma, N. *ACS Appl. Mater. Interfaces* **2013**, *5*, 1149−1155.
(14) Fitzmorris, B. C.; Pu, Y.-C.; Jason, K.; Cooper, J. K.; Lin, Y.-F.; Hsu, Y.-J.; Li, Y.; Zhang, J. Z. *ACS Appl. Mater. Interfaces* **2013**, *5*, 2893−2900.
(15) Zhu, G.; Xu, Z. *J. Am. Chem. Soc.* **2011**, *133*, 148−157.
(16) Shen, S.; Zhang, Y.; Peng, L.; Du, Y.; Wang, Q. *Angew. Chem., Int. Ed.* **2011**, *50*, 7115−7118.
(17) Han, W.; Yi, L.; Zhao, N.; Tang, A.; Gao, M.; Tang, Z. *J. Am. Chem. Soc.* **2008**, *130*, 13152−13161.
(18) Shen, S.; Zhang, Y.; Liu, Y.; Peng, L.; Chen, X.; Wang, Q. *Chem. Mater.* **2012**, *24*, 2407−2413.
(19) Xiao, C.; Xu, J.; Li, K.; Feng, J.; Yang, J.; Xie, Y. *J. Am. Chem. Soc.* **2012**, *134*, 4287−4293.
(20) Yan, R.; Gargas, D.; Yang, P. *Nat. Photonics* **2009**, *3*, 569−576.
(21) Shen, H.; Wang, H.; Tang, Z.; Niu, J. Z.; Lou, S.; Du, Z.; Li, L. S. *CrystEngComm* **2009**, *11*, 1733−1738.
(22) Shen, H.; Wang, H.; Li, X.; Niu, J. Z.; Wang, H.; Chen, X.; Li, L. S. *Dalton Trans.* **2009**, *47*, 10534−10540.
(23) Shen, H.; Zhou, C.; Xu, S.; Yu, C.; Wang, H.; Chen, X.; Li, L. S. *J. Mater. Chem.* **2011**, *21*, 6046−6053.
(24) Ryan, K. M.; Mastroianni, A.; Kimani, A.; Stancil, K. A.; Liu, H.; Alivisatos, A. P. *Nano Lett.* **2006**, *6*, 1479−1482.
(25) Kronik, L.; Shapira, Y. *Surf. Sci. Rep.* **1999**, *37*, 1−20.
(26) Baikie, I.; Petermann, U.; Lagel, B. *Surf. Sci.* **1999**, *433−435*, 249−253.
(27) Lagel, B.; Baikie, I. D.; Petermann, U. *Surf. Sci.* **1999**, *433−435*, 622−626.
(28) Li, L. S.; Zhang, J.; Wang, L. J.; Chen, Y.; Hui, Z.; Li, T. J.; Chi, L. F.; Fuchs, H. J. *Vac. Sci. Technol. B* **1997**, *15*, 1618−1622.
(29) Li, A. D. Q.; Li, L. S. *J. Phys. Chem. B* **2004**, *108*, 12842−12850.
(30) Li, L. S.; Jia, Q. X.; Li, A. D. Q. *Chem. Mater.* **2002**, *14*, 1159−1165.
(31) Sahu, A.; Qi, L.; Kang, M. S.; Deng, D.; Norris, D. J. *J. Am. Chem. Soc.* **2011**, *133*, 6509−6512.